Time-Resolved Study of Crystallization in Deeply Cooled Liquid Parahydrogen

Matthias Kühnel,[1] José M. Fernández,[2] Guzmán Tejeda,[2] Anton Kalinin,[1] Salvador Montero,[2] and Robert E. Grisenti[1,3,*]

[1]*Institut für Kernphysik, J. W. Goethe-Universität, Max-von-Laue-Strasse 1, 60438 Frankfurt am Main, Germany*
[2]*Laboratory of Molecular Fluid Dynamics, Instituto de Estructura de la Materia, CSIC, Serrano 121, 28006, Madrid, Spain*
[3]*GSI Helmholtzzentrum für Schwerionenforschung, Planckstrasse 1, 64291 Darmstadt, Germany*

(Received 13 April 2011; revised manuscript received 17 May 2011; published 14 June 2011)

We present real-time measurements of the crystallization process occurring in liquid para-hydrogen (para-H_2) quenched to $\approx 0.65T_m$ ($T_m = 13.8$ K is the melting point of bulk liquid para-H_2). The combination of high spatial resolution Raman spectroscopy and liquid microjet generation allows, *in situ*, capturing structural changes with $\sim 10^{-8}$ s time resolution. Our results provide a crystal growth rate that rules out a thermally activated freezing process and reveal that the quenched melt freezes into a metastable polymorph, which undergoes a structural transition. The achieved temporal control offers new opportunities for exploring the elementary processes of nonequilibrium phase transformations in supercooled liquids.

DOI: 10.1103/PhysRevLett.106.245301 PACS numbers: 67.63.Cd, 33.20.Fb, 64.60.My, 64.70.dg

Crystallization processes play a fundamental role in many areas of condensed matter science, yet the underlying mechanisms are not fully understood [1]. A major experimental challenge is to directly inspect the phase change dynamics, especially in liquids cooled significantly below their normal melting point where crystallization normally proceeds very rapidly. Understanding phase transformations in supercooled liquids might help in elucidating the nature of the liquid-glass transition [2]. In addition, it would be important from the applied point of view, as solidification from a quenched melt provides the route to directly control the structure and physical properties in a great number of materials [3]. So far, however, detailed studies of crystallization in deeply cooled liquids have proven challenging, and our current knowledge primarily comes from extensive computational work [4–8]. Recent experimental efforts have focused on the investigation of crystallization in quenched metallic melts [9–12], but these studies either lack the capability of time-resolving structural changes or are limited to time scales of the order of 1 s at the shortest.

In this Letter, we present an experimental approach that allows *in situ* spectroscopic investigation of the phase change dynamics in a deeply cooled liquid on the submicrosecond time scale. To demonstrate the potential of our concept we provide insights into the crystallization process in deeply cooled para-H_2.

We choose para-H_2, the molecular species characterized by a total nuclear spin equal to zero [13], as a model system because of its unique properties. Hydrogen is the simplest of all molecular species, albeit quantum effects dominate the properties of the condensed phases [13,14]. Below 20 K only the $J = 0$ rotational state is populated [14], and hence at low temperatures para-H_2 is a spinless boson. As such, para-H_2 was suggested as the next ideal candidate, in addition to the helium isotopes, that might exhibit superfluidity [15]. At present, there is only indirect evidence for superfluidity coming from spectroscopic studies of doped tiny para-H_2 clusters [16,17]. With a transition temperature estimated around $0.2T_m$ [18], extensive supercooling represents the major experimental obstacle in observing superfluidity of para-H_2. The question about a superfluid transition in bulk liquid para-H_2 is thus ultimately related to the more general topic concerning the possible existence in supercooled liquids of a metastability limit, below which crystallization would become unavoidable. There is numerical evidence that such a limit exists [6,19], but to what extent the reported conclusions apply to para-H_2 is an open question. Recent experiments suggest that para-H_2 clusters may remain liquid at temperatures down to $\approx 0.4T_m$ [20,21], but substantial supercooling in the bulk has not been achieved so far [22].

The spherical symmetry of the para-H_2 rotational ground state results in a highly isotropic intermolecular interaction that can be modeled by a Lennard-Jones potential [13,14]. Liquid para-H_2 represents thus the quantum analogue of conceptually simple liquids such as argon that are routinely quenched in computer simulations [4–8]. On the experimental side, predicted crystallization rates as high as $\sim 10^2$ cm s^{-1} [2,4] have so far prevented the study of these prototype model systems. Our results provide a quantitative test of molecular dynamics investigations of crystallization in deeply cooled liquids.

Figure 1(a) shows the experimental setup. To produce deeply cooled para-H_2 we expand in a laminar flow the pressurized liquid through a 5.2 ± 0.5 μm-diameter capillary orifice into a high-vacuum chamber. Liquid para-H_2 with less than 0.6% ortho concentration is produced by continuous catalytic conversion from 99.9999% purity natural H_2 [23]. The liquid emerges as a continuous cylindrical filament that rapidly cools by surface evaporation at an expected maximum rate exceeding 10^7 K s^{-1} [24], before it starts freezing by homogeneous crystal nucleation [25]. We point out that the severe problem of heterogeneous

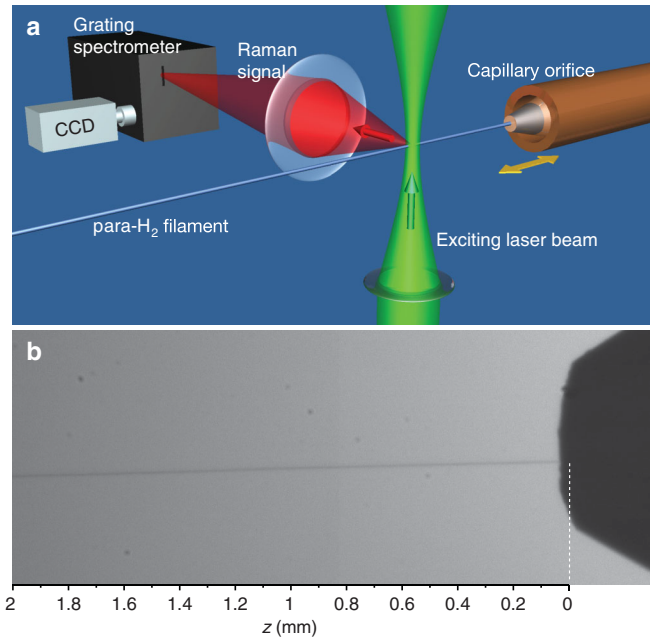

FIG. 1 (color). (a) Schematic view of the experimental setup (see the text). (b) Shadow image [24] of the continuous para-H_2 filament produced at a nominal source pressure of ≈ 14 bar and a source temperature of ≈ 15.8 K. The white dashed line indicates the zero position of the glass capillary orifice, which is located about 30 μm to the right of the dark capillary edge visible in the image.

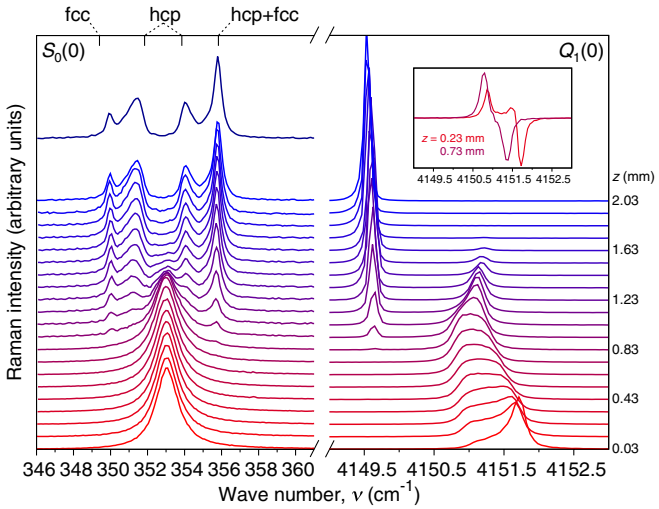

FIG. 2 (color online). Selected Raman spectra of the rotational $S_0(0)$ (left) and vibrational $Q_1(0)$ (right) transitions recorded between $z \approx 0.03$ mm and $z \approx 2.03$ mm. The uppermost rotational spectrum was measured further downstream from the orifice at $z \approx 2.53$ mm. The inset shows two examples of derivatives of vibrational spectra, whose outermost maxima and minima wave numbers define the temperatures of the coldest and hottest filament regions, respectively, by taking into account the spectral resolution. The top-axis vertical ticks in the left panel indicate the wave numbers of the experimental hcp [26] and theoretical fcc [14] rotational lines in bulk solid para-H_2.

nucleation sites is greatly suppressed by the clean, continuously replenishing vacuum-exposed jet surface. The shape and flow conditions of the liquid jet are monitored by shadow imaging techniques [24], as shown in Fig. 1(b). The filament has a pointing stability of better than 1 μm about 1 mm downstream from the orifice.

Insight into phase change dynamics is obtained by recording Raman spectra of the rotational $S_0(0)$ and vibrational $Q_1(0)$ transitions [21,26] as a function of the distance z from the orifice. Raman scattering is excited by a single mode cw Ar^+ laser beam focused down to a diameter of ≈ 14 μm onto the filament. The Raman signal, which is proportional to the molecular number density, is collected at 90° with respect to both the laser beam and filament axis and is focused onto the 20 μm entrance slit of the grating spectrometer [27], equipped with a CCD detector cooled by liquid nitrogen. The spectral resolution is ≈ 0.11 cm^{-1} at 4150 cm^{-1} and ≈ 0.24 cm^{-1} at 350 cm^{-1}. The probed filament volume is selected by axial displacement of the nozzle assembly with an accuracy of better than 1 μm. The temporal axis in our experimental setup is defined by $t = z/v_{\mathrm{jet}}$, where the jet velocity $v_{\mathrm{jet}} \approx 118 \pm 20$ m s^{-1} is determined by mass flow measurements; in particular, the overall experimental spatial resolution of ≈ 2 μm along the filament turns into a time resolution of ≈ 17 ns.

Figure 2 displays selected rotational (left panel) and vibrational (right panel) Raman spectra recorded between $z \approx 0.03$ mm and $z \approx 2.03$ mm. At the closest distance the vibrational spectrum consists of a strongly asymmetric band with its peak centered at $\nu \approx 4151.7$ cm^{-1}, which corresponds to bulk liquid para-H_2 at ≈ 16.8 K. The filament temperature is determined from the reported dependence of the vibrational wave number on liquid temperature, $\nu(T)$ [21], extrapolated for $T < T_m$. In Fig. 3, we plot the average filament temperature as a function of z (purple symbols), which illustrates the rapid cooling of the expanding liquid filament. The temperature increase seen for $z > 0.9$ mm is accompanied by the appearance in the vibrational spectrum of a second, rapidly growing sharp line at $\nu \approx 4149.6$ cm^{-1} corresponding to solid para-H_2 [21,26] and thus results from the heat released during the initiated solidification process. The broad shape of the liquid vibrational band, especially seen during early propagation times (Fig. 2), is the signature of a temperature gradient across the liquid stream. This is illustrated more explicitly in Fig. 3 by the large temperature gap for $z < 1$ mm between the hottest (red circles) and coldest (blue circles) regions of the expanding filament, which correspond to the two extreme inflection-point wave numbers in the vibrational band of the liquid (see the inset in Fig. 2).

The radial temperature gradient results from the finite thermal conductivity of liquid hydrogen. To show this, we simulate the jet cooling by dividing the filament into 100 equally mass-weighted cylindrical layers. We allow for evaporative cooling [24] of the outermost layer, whereas the heat transfer between any two neighboring layers governs the temperature change in the interior. The computed

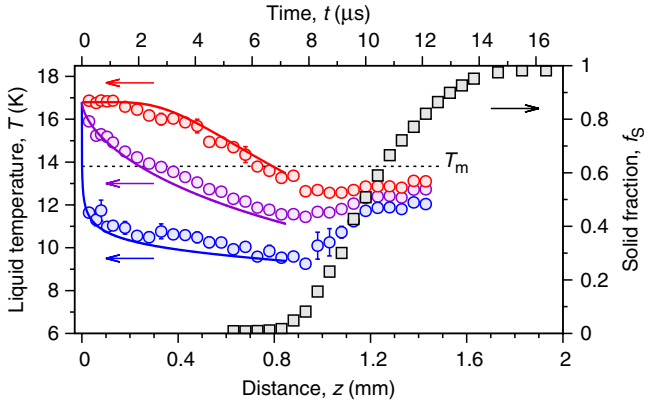

FIG. 3 (color online). Experimental liquid filament temperatures (circles, left y axis) and solid fraction f_S (squares, right y axis) extracted from the vibrational spectra of Fig. 2. The purple circles represent the average temperature, whereas the red and blue symbols illustrate the highest and lowest temperatures, respectively. The solid lines are numerical simulation results of the cooling process (see the text). The dashed line marks the melting point of bulk liquid para-H_2. The time axis is defined as $t = z/v_{\mathrm{jet}}$, where v_{jet} is the jet velocity.

filament temperature averaged over the entire volume and the temperatures of the inner core and surface layer are shown in Fig. 3 as purple, red, and blue solid lines, respectively. The agreement with the experimental data also confirms the deep quenching to about 9 K ($\approx 0.65T_m$) of a fraction of the expanding liquid filament. The steep increase of the filament surface temperature for $z > 0.9$ mm suggests that the crystallization front initiates at the cold surface and proceeds inwards. This is further confirmed by additional vibrational Raman spectra measured transversely to the filament axis at $z = 0.8$ mm at a higher spatial resolution, which show that the solid fraction at the filament edge ($\approx 10\%$) is larger than at the center ($< 2\%$).

The time evolution of the solid fraction, shown in Fig. 3, allows us to estimate the rate of linear crystal growth u, which is the fundamental physical quantity governing the kinetics of crystallization [25]. A lower limit for the growth rate is readily obtained by dividing the filament radius (≈ 2.6 μm) by the total freezing time (≈ 8 μs) (Fig. 3), yielding $u \approx 33$ cm s^{-1}. A more accurate determination of the growth rate is difficult because the crystal nucleation rate for para-H_2 is not known with sufficient precision [28].

According to the kinetic theory, the rate of crystal growth can be written in terms of the rate u_0 at which the molecules leave the melt and join the solid [4,25]:

$$u = f u_0 \exp(-m\Delta h/kT_m)[1 - \exp(-m\Delta g/kT)], \quad (1)$$

where m is the mass of the hydrogen molecule, k is the Boltzmann constant, Δh is the enthalpy of fusion, $f \leq 1$ is the fraction of active sites that contribute to the growth, and $\Delta g(T)$ is the difference in free energy (per unit mass) of liquid and solid para-H_2. The latter can be computed from the experimental equilibrium heat capacity data for the liquid, extrapolated for $T < T_m$, $c_L(T) = A_2 T$ [28], with $A_2 \approx 466$ J kg^{-1} K^{-2}, and for the solid, fitted to $c_S(T) = AT^3 + BT^5$ [28], with $A \approx 0.815$ J kg^{-1} K^{-4} and $B \approx 0.001\,37$ J kg^{-1} K^{-6}. If the crystallization process is thermally activated, as experimentally observed in a variety of melts, including quenched monatomic metallic liquids [12], the characteristic rate is given by $u_0 = D/a$ [4], where D is the liquid diffusion constant and a is a typical interatomic distance that can be written as $a \approx n_L^{-1/3}$, with n_L the liquid number density. The liquid diffusion constant is written in the Arrhenius form $D = D_0 \exp(-E/kT)$ [25], where $D_0 \approx 10^{-4}$ cm^2 s^{-1} and $E/k \approx 46$ K for liquid para-H_2. Even by assuming the (unrealistic) value $f = 1$ [4,25], the resulting theoretical growth rate of $u \approx 0.9$ cm s^{-1}, computed for $T = 9.5$ K (see Fig. 3), is smaller by about 2 orders of magnitude than the above estimate of u from our experimental data.

Broughton, Gilmer, and Jackson [4] performed molecular dynamics simulations of the crystal growth from a Lennard-Jones melt and found that their computed rates could be well reproduced by the kinetic model [Eq. (1)] with the characteristic rate determined by the average thermal velocity, $u_0 = (3kT/m)^{1/2}$. We find that our experimental lower limit for the growth rate in para-H_2 is consistent with the collision-limited model if we assume the more realistic $f = 0.01$.

Additional insights into the crystallization process come from the analysis of the rotational spectra (Fig. 2). For $z < 0.7$ mm they present a single broad line centered at $\nu \approx 353$ cm^{-1}, as in the bulk liquid [21,26]. As the filament starts freezing, additional features appear. The rotational Raman spectrum of bulk solid para-H_2 consists of either three lines, corresponding to the hexagonal closed-packed (hcp) crystal structure, or two lines, which correspond to the face-centered cubic (fcc) structure [14]. Solid para-H_2, when grown from the melt, is always found to be hcp [13], which is the energetically favored crystal structure. However, our spectra clearly evidence four peaks, which agree with both the hcp and fcc structures, indicating that the crystal rapidly grows into a metastable polymorph, probably the random hexagonal closed-packed (rhcp) phase, a random mixture of hcp and fcc domains [29]. This phenomenon of crystal phase selection [5,7,8,29] is consistent with Ostwald's conjecture, which states that the crystal phase that nucleates from the melt is that with the lowest energy barrier. Indeed, the formation of critical rhcp nuclei in deeply cooled liquid para-H_2 should be favored by the similar free energies of the hcp and fcc phases [13]. Rotational spectra evidencing both hcp and fcc structures have also been measured in solid layers grown by deposition of para-H_2 gas at $T < 4$ K, though with noticeable differences in the relative intensities compared to ours [30,31].

Careful inspection of the rotational spectra reveals that the relative intensities of the solid peaks change with propagation time. In Fig. 4, we plot the relative peak area f_{fcc} of the fcc line at $\nu \approx 350$ cm^{-1} with respect to the hcp line at $\nu \approx 351.2$ cm^{-1}, which we choose as a measure of

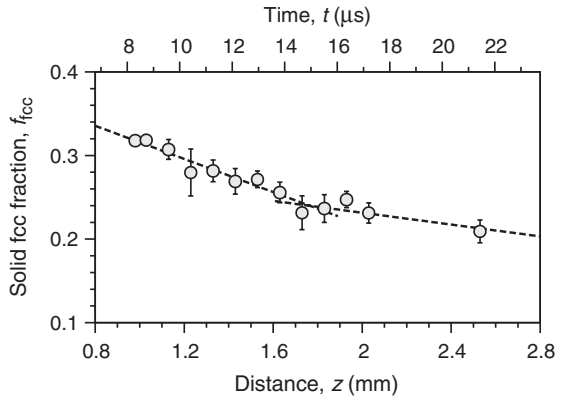

FIG. 4. Relative peak area f_{fcc} (symbols) of the fcc rotational line at $\nu \approx 350\ cm^{-1}$ with respect to the hcp line at $\nu \approx 351.2\ cm^{-1}$ (Fig. 2). The areas are determined by fitting the experimental rotational lines to pseudo-Voigt functions. The dashed lines are guides to the eye emphasizing the slight change in the transformation rate at $z \approx 1.8$ mm, which roughly marks the end of freezing process (Fig. 3).

the fcc solid fraction in the experimentally probed volume. The observed decrease of f_{fcc} for $z > 1.8$ mm, after the freezing process has completed (Fig. 3), hints at a spontaneous transformation of the rhcp phase into the thermodynamically stable hcp crystal structure. Whereas there is numerical evidence that structural transitions play a critical role during the nucleation step [5,7,8], our results clearly indicate that crystal phase selection lasts a significant fraction of the growth process. The slightly higher transformation rate for $z < 1.8$ mm is attributed to the adsorption of a larger amount of para-H_2 molecules on the hcp (than fcc) facets of the growing crystal [7]; the temperature increase accompanying the solidification process (Fig. 3) might also contribute to the observed faster decrease of f_{fcc} [30].

The high cooling rates combined with the ability to time-resolve fast structural changes as demonstrated in the present work open the way to novel studies of nonequilibrium liquid-solid phase transitions in deeply cooled liquids. Extensions of our work can be anticipated and include enhancing the cooling of the filament, which can be achieved by injecting the liquid jet into a cold helium-gas atmosphere [24]. This concept will enable the exploration of phase transformations at deeper quenches, providing a way to directly control the filament temperature. Increasing the cooling rate should also allow investigating phase transitions in liquids characterized by a low vapor pressure at melting, which results in less efficient evaporative cooling upon expansion into vacuum than for the para-H_2 filament. Preliminary experiments with jets of liquid nitrogen and oxygen clearly evidence the breakup of the filament into droplets as a result of Rayleigh-induced oscillations, indicating that the time for crystal nucleation is higher than our typical observation time (Fig. 3). Experiments with H_2 jets of different ortho-H_2 concentration that aim at elucidating the role played by anisotropic interactions in the nucleation process, especially with respect to the extent of supercooling [22], are currently in progress. Last, our approach offers the possibility to experimentally address the predicted transition to a structural quantum glass in a supercooled liquid mixture of para-H_2 and ortho-D_2 [32].

We acknowledge financial support from the Helmholtz Gemeinschaft, through Grant No. VH-NG-331, and the Spanish Ministerio de Ciencia e Innovacion, through Grants No. FIS2010-22064-C02-01 and No. HD2008-0068. We acknowledge travel support from the German academic exchange service (DAAD) under reference No. 50025171.

*grisenti@atom.uni-frankfurt.de

[1] D. W. Oxtoby, Nature (London) **347**, 725 (1990).
[2] D. Turnbull, Contemp. Phys. **10**, 473 (1969).
[3] F. Spaepen, Science **235**, 1010 (1987).
[4] J. Q. Broughton, G. H. Gilmer, and K. A. Jackson, Phys. Rev. Lett. **49**, 1496 (1982).
[5] P. R. Ten Wolde *et al.*, J. Chem. Phys. **104**, 9932 (1996).
[6] F. Trudu, D. Donadio, and M. Parrinello, Phys. Rev. Lett. **97**, 105701 (2006).
[7] J.-M. Leyssale *et al.*, J. Chem. Phys. **122**, 104510 (2005).
[8] C. Desgranges and J. Delhommelle, Phys. Rev. Lett. **98**, 235502 (2007).
[9] J. Y. Tsao *et al.*, Phys. Rev. Lett. **56**, 2712 (1986).
[10] R. Willnecker, D. M. Herlach, and B. Feuerbacher, Phys. Rev. Lett. **62**, 2707 (1989).
[11] C. Notthoff *et al.*, Phys. Rev. Lett. **86**, 1038 (2001).
[12] W.-L. Chan *et al.*, Phys. Rev. Lett. **102**, 095701 (2009).
[13] I. F. Silvera, Rev. Mod. Phys. **52**, 393 (1980).
[14] J. V. Kranendonk, *Solid Hydrogen* (Plenum, New York, 1983).
[15] V. L. Ginzburg and A. A. Sobyanin, JETP Lett. **15**, 242 (1972).
[16] S. Grebenev *et al.*, Science **289**, 1532 (2000).
[17] H. Li *et al.*, Phys. Rev. Lett. **105**, 133401 (2010).
[18] V. S. Vorob'ev and S. P. Malysehnko, J. Phys. Condens. Matter **12**, 5071 (2000).
[19] A. Cavagna, A. Attanasi, and J. Lorenzana, Phys. Rev. Lett. **95**, 115702 (2005).
[20] K. Kuyanov-Prozument and A. F. Vilesov, Phys. Rev. Lett. **101**, 205301 (2008).
[21] R. Sliter and A. F. Vilesov, J. Chem. Phys. **131**, 074502 (2009).
[22] H. J. Maris, G. M. Seidel, and F. I. B. Williams, Phys. Rev. B **36**, 6799 (1987).
[23] G. Tejeda *et al.*, J. Chem. Phys. **128**, 224308 (2008).
[24] R. E. Grisenti *et al.*, Europhys. Lett. **73**, 540 (2006).
[25] K. A. Jackson, *Kinetic Processes* (Wiley, Weinheim, 2004).
[26] S. S. Bhatnagar *et al.*, Can. J. Phys. **40**, 9 (1962).
[27] G. Tejeda *et al.*, Appl. Spectrosc. **51**, 265 (1997).
[28] H. J. Maris *et al.*, J. Low Temp. Phys. **51**, 471 (1983).
[29] S. Auer and D. Frenkel, Nature (London) **409**, 1020 (2001).
[30] G. W. Collins *et al.*, Phys. Rev. B **53**, 102 (1996).
[31] M. E. Fajardo and S. Tam, J. Chem. Phys. **108**, 4237 (1998).
[32] E. Rabani and D. R. Reichman, Annu. Rev. Phys. Chem. **56**, 157 (2005).